SERS as a bioassay platform: fundamentals, design, and applications

Marc D. Porter,*[a] Robert J. Lipert,*[b] Lorraine M. Siperko,[a] Gufeng Wang[b] and Radha Narayanan[a]

Received 15th January 2008
First published as an Advance Article on the web 18th March 2008
DOI: 10.1039/b708461g

Bioanalytical science is experiencing a period of unprecedented growth. Drivers behind this growth include the need to detect markers central to human and veterinary diagnostics at ever-lower levels and greater speeds. A set of parallel arguments applies to pathogens with respect to bioterrorism prevention and food and water safety. This *tutorial review* outlines our recent explorations on the use of surface enhanced Raman scattering (SERS) for detection of proteins, viruses, and microorganisms in heterogeneous immunoassays. It will detail the design and fabrication of the assay platform, including the capture substrate and nanoparticle-based labels. The latter, which is the cornerstone of our strategy, relies on the construction of gold nanoparticles modified with both an intrinsically strong Raman scatterer and an antibody. This labelling motif, referred to as extrinsic Raman labels (*ERLs*), takes advantage of the well-established signal enhancement of scatterers when coated on nanometre-sized gold particles, whereas the antibody imparts antigenic specificity. We will also examine the role of plasmon coupling between the *ERLs* and capture substrate, and challenges related to particle stability, nonspecific adsorption, and assay speed.

Overview of SERS as an analytical tool

A host of immunoassay detection techniques have been developed in past years. The more established approaches rely on scintillation counting, fluorescence, electrochemistry, and enzymatic amplification.[4] This paper reviews our ongoing studies on the merits of surface enhanced Raman scattering (SERS) as a rapid, sensitive tool for assay readout.

As historically traced and mechanistically detailed in other contributions to this special issue of *Chemical Society Reviews*, traditional forms of Raman spectroscopy lack the sensitivity required of a readout strategy.[5] Research in the 1970s led to the discovery of a surface effect, now known as SERS, in which the scattering of pyridine and similar compounds was markedly enhanced when adsorbed on roughened silver surfaces.[6,7] Recent work with silver nanoparticles as enhancing substrates has shown that SERS can be applied to single molecule detection,[8,9] rivalling the performance of fluorescence measurements.

The basis of SERS rests in the use of roughened, coinage metal surfaces to amplify scattering.[10–13] The observed enhancement (up to 10^{14} times[11]) is attributed to two effects: chemical and electromagnetic. The chemical component is based on the formation of a charge-transfer state between the metal and adsorbed scatterer,[14] and contributes about two orders of magnitude to the overall enhancement. The electromagnetic effect arises from the collective oscillation of conduction electrons that results when a metal is irradiated with light. This process, known as surface plasmon resonance, has a

[a] *Departments of Chemistry, Chemical Engineering and Bioengineering, University of Utah, Salt Lake City, UT 84018, USA. E-mail: marc.porter@utah.edu; Fax: +1-801-585-0575; Tel: +1-801-587-1505*
[b] *Institute for Combinatorial Discovery and the Ames-Laboratory-USDOE, Iowa State University, Ames, IA 50014, USA. E-mail: blipert@ameslab.gov; Fax: +1-515-294-0062; Tel: +1-515-294-8837*

Robert J. Lipert received his PhD in chemistry from Yale University and is currently with the Institute for Combinatorial Discovery at Iowa State University. His research interests center on the application of lasers to chemical analysis.

Lorraine M. Siperko received her PhD from The Ohio State University. Her career has encompassed industrial and academic research in the general area of surface and interfacial interactions. She is presently a Senior Research Scientist in the Center for Nanobiosensors at the University of Utah. Her current research interests include surface spectroscopies and scanning probe microscopic imaging.

Gufeng Wang received his BS from Nanjing University, China in 1995. He obtained his PhD in analytical chemistry from the University of Iowa in 2004. He is currently a postdoctoral associate in Iowa State University. His research focuses on developing fast, sensitive and high-throughput detection platforms for cancer markers, pathogens and biowarfare agents.

Radha Narayanan obtained her PhD in analytical chemistry in May 2005 under the direction of Mostafa A. El-Sayed at the Georgia Institute of Technology. She is a postdoctoral fellow for Marc D. Porter and will be an assistant professor at the University of Rhode Island from July 2008. Her research interests are synthesis of metal nanoparticles for environmental, catalytic, and biological applications.

wavelength dependence tied to the nanometric roughness and identity of metallic surfaces and, as reported recently, the size and shape of nanoparticles.[15]

Detection by SERS has several potentially valuable attributes with respect to the noted signal transduction methods.[16] First, when employing gold nanoparticles, excitation in the red spectral region is used, which minimizes possible interference from native fluorescence. Second, Raman processes are less susceptible to photobleaching, enabling the use of signal averaging to increase sensitivity and lower detection levels. Finally, the widths of Raman spectral bands are 10–100 times narrower than those of fluorescence, which reduces the potential for spectral overlap from multiple labels and thus facilitates multiplexed applications.

Early attempts to capitalize on SERS in ultrasensitive chemical analysis, however, were hampered by difficulties in fabricating surfaces with reproducible enhancements. This situation has changed with recent breakthroughs in the technical ability to controllably and reproducibly synthesize nanoparticles and other nanometric objects with a predetermined size and shape.[17,18] These developments have triggered a renewed interest in the exploration of this information rich spectroscopy as a tool for rapid, low-level readout,[19,20] especially, and as featured in contributions throughout this special issue, in the area of chip scale bioassays.[16,19–29]

There is one more important technological advancement: the transformation of instrumentation requisite for high sensitivity Raman spectroscopy. Not many years ago, these measurements required large, expensive laboratory hardware that consisted of high power lasers, double and triple monochromators, specialized detectors, and vibrational isolation systems. Today, advances in optical filters, array detectors, and fiber optics have moved Raman spectroscopy from the controlled surroundings of the analytical laboratory to the industrial plant floor and other demanding environments. These developments also markedly reduced equipment and labor costs, while maintaining a remarkably high level of performance in a rugged, field-deployable instrument. Based on the collective weight of these innovations, we believe that the next decade will witness the widespread deployment of Raman spectroscopy into areas previously not imagined. The following details our efforts aimed at translating SERS to the bioassay arena.

Immunoassays *via* SERS

As outlined in Scheme 1, there are three key components in our SERS-based immunoassay platform: (1) use of a capture substrate to specifically extract and concentrate antigens from solution; (2) selective tagging of captured antigens with functionalized gold nanoparticles; and (3) readout by Raman spectroscopy.[16,25] The antigen is therefore selectively sandwiched between a gold surface and gold nanoparticles by the capture and labelling antibodies. As scaled roughly by size in Fig. 1, we have applied this approach to the detection of immunoglobulin G,[16] free prostate specific antigen (f-PSA),[25] viral pathogens,[24] and simulants of biowarfare agents.[26] These works have shown that this format not only offers low levels of detection (*e.g.*, ~30 fM for f-PSA in human serum) but can also record single-binding events on a capture substrate.[30] This section details the three components of the platform.

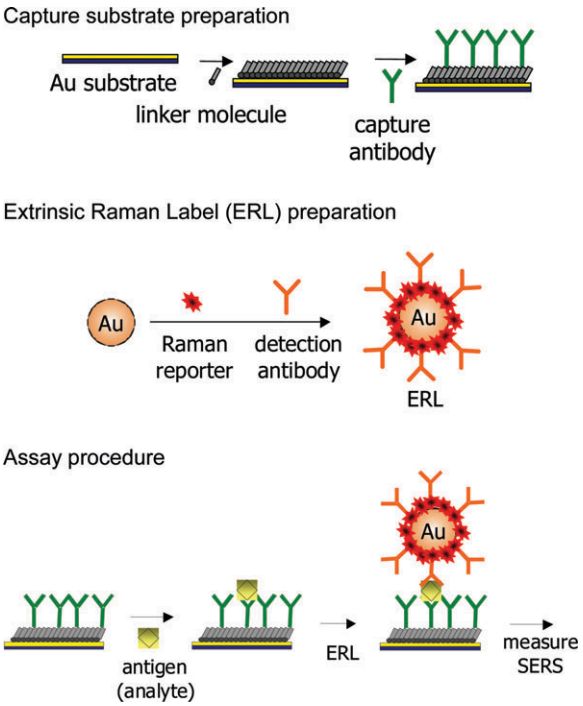

Scheme 1 SERS-based immunoassay platform.

Preparation of capture substrates

The capture substrate uses a coupling agent that forms a gold-bound thiolate and can covalently couple with the primary amines on antibodies for immobilization. Its preparation starts with the gold substrate, which, for us, entails the construction of template-stripped gold (TSG).[31] TSG has a sub-nanometre surface roughness, making it well suited for measuring the size, shape, and density of nanometric objects (*e.g.*, viruses and colloidal gold) by atomic force (AFM) and scanning electron (SEM) microscopies. These characterizations provide an important means for performance validation by correlations with the SERS response. TSG was prepared by resistively evaporating ~250 nm of gold (99.9% purity) at a rate of 0.1 nm s^{-1} onto a 10.2 cm p-type silicon [111] wafer

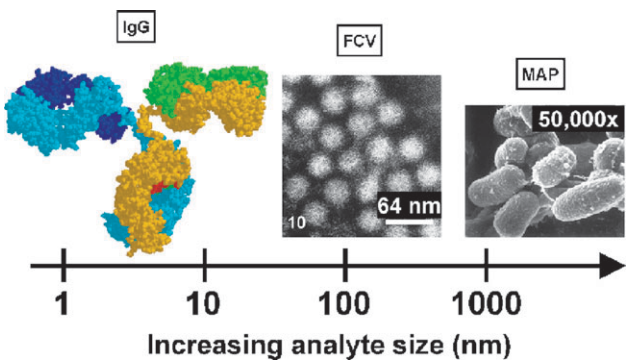

Fig. 1 Size scale of possible antigens in heterogeneous immunoassays: immunoglobulin G (IgG),[1] feline calicivirus (FCV),[2] and *Mycobacterium avium* subsp. *paratuberculosis* (MAP).[3] Reprinted with permission from ref. 1–3.

(University Wafer) with an Edwards 306A resistive evaporator. Glass microscope slides were cut into 1 × 1 cm squares and ultrasonically bathed in diluted Contrad 70 (Micro, Cole-Parmer), deionized water, and ethanol, each for 30 min. The clean glass chips were affixed to the gold-coated wafer with 2-part epoxy (Epoxy Technology) and cured at 150 °C for 1.75 h. The glass chips were then gently detached from the silicon wafer, which removes the sandwiched gold film, to yield a smooth gold surface on the topside of the glass chip.

The next step creates a small address to minimize sample volume and reagent consumption. For this, soft lithography[24] was used to surround a 3 mm diameter area of uncoated gold with a hydrophobic octadecanethiolate adlayer, which confines small liquid droplets. This substrate was submerged in an ethanolic solution of dithiobis(succinimidyl undecanoate) (DSU) or dithiobis(succinimidyl propionate) (DSP) to form a thiolate adlayer on the uncoated gold address that can also covalently tether proteins and other amine-containing substances by amide linkages. Construction is completed by exposure to a buffered solution of capture antibody in a humidity chamber, followed by treatment with a blocking agent such as bovine serum albumin (BSA). This step "caps" any residual succinimidyl groups. Other blockers (*e.g.*, human serum albumin (HSA) and evaporated milk) have also been used, with selection based on a panel of trial-and-error tests.

There are two issues with this preparation that require further consideration: the efficiency of the coupling reaction; and the activity of the immobilized antibodies.

Characterization of capture substrates

Infrared reflection spectroscopy (IRS) has been used to examine the first concern. These findings are presented in Fig. 2 and 3. Fig. 2 presents IRS data diagnostic of DSP- and DSU-derived monolayers chemisorbed to gold.[32,33] The bands at 1817, 1788, and 1751 cm^{-1} arise from the C=O stretch of the ester, and the respective in-phase and out-of-phase C=O stretches of the succinimidyl end group.[34] The bands at 1218 cm^{-1} (C–N–C stretch) and 1077 cm^{-1} (N–C–O stretch) are also succinimidyl group markers. Although not apparent at the *y*-axis scale of the spectra, the results also show that the positions of the symmetric and asymmetric C–H stretching modes (2850–2925 cm^{-1}) for the two adlayers are slightly different. The methylene stretching modes for the longer chain coupler are slightly lower in energy (4–7 cm^{-1}) than those for the shorter chain analogue, suggesting the latter adlayer is more disordered than the former adlayer.[35]

IRS was also used to investigate the hydrolysis rates of the succinimidyl groups on the immobilized modifiers. This measurement is important because the hydrolysis of the ester competes with protein coupling. The rate of hydrolysis was therefore monitored *via* the change in the succinimidyl band at 1751 cm^{-1} as a function of exposure time to borate buffer (pH 8.5). The results are shown in Fig. 3A. The decrease in band strength is indicative of succinimidyl hydrolysis. The data indicate that hydrolysis for the short chain system proceeds much more rapidly, requiring ~5 h for completion. These results are consistent with earlier reports showing that the rate of ester hydrolysis is strongly influenced by monolayer packing density and linker orientation.[36,37]

To assess antibody coupling, the rate of protein A binding was monitored by following the growth of the amide band at 1665 cm^{-1} at each adlayer. These data are plotted in Fig. 3B. Comparison of the two profiles indicates that not only the rate of protein binding differs, but also that binding at the shorter chain system is ~40% more effective. We believe that the higher binding level reflects the lower packing density, and therefore greater flexibility, of the DSP-derived adlayer. In this

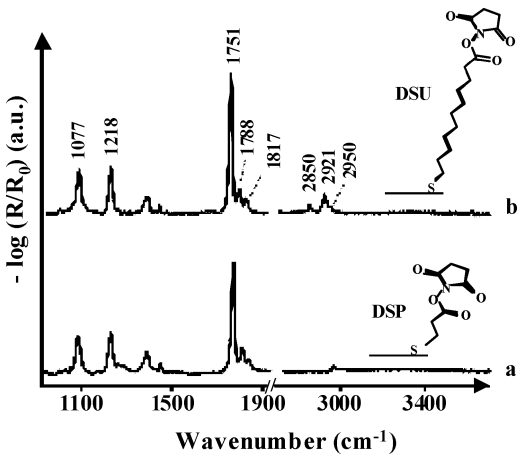

Fig. 2 IRS of (a) DSP- and (b) DSU-derived monolayers on gold. Reproduced with permission from ref. 32.

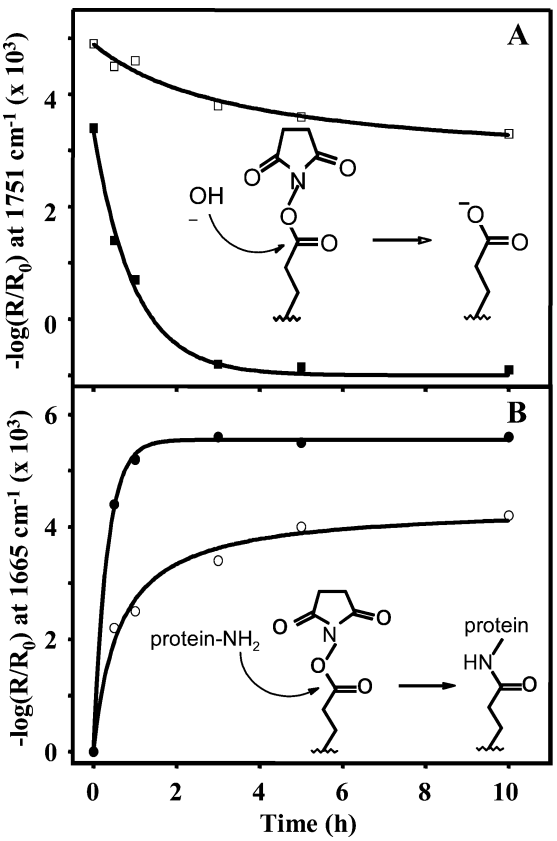

Fig. 3 Reactivity of adlayers derived at gold from DSU and DSP: (A) hydrolysis of DSU (□) DSP (■); (B) binding of protein A by DSP (●) DSU (○). Reproduced with permission from ref. 32.

case, both the uptake of protein A and the terminal group hydrolysis are completed in ~3 h, which though not tested, suggests blocking residual terminal groups may not be necessary.

One more issue should be addressed: the activity of the immobilized antibodies. Work in the Shannon laboratory used AFM to gauge this issue.[38] Results indicated that ~30% of the immobilized IgG antibodies were effective in antigen binding. This level of activity was attributed to steric effects with respect to the spatial orientation of the capture antibody and/or to interactions with the adlayer causing protein denaturation. Moreover, the distribution of lysine residues throughout the IgG structure argues that an immobilized antibody can have a distribution of orientations. These data point to the possible improvement in the level of detection by employing synthetic routes that would engender a more favorable spatial orientation for the immobilized antibody. The improvement, however, would at best be a factor of 2–3.

Design, synthesis, and characterization of extrinsic Raman labels

Design. Our assays use extrinsic Raman labels (*ERLs*) to quantitatively take advantage of amplified scattering.[16,24–26,30,39–42] *ERLs* exploit the intrinsically strong Raman scattering of aromatic compounds (*i.e.*, reporters). The reporters are deposited on the gold nanoparticles, along with a coating of a molecular recognition element (*e.g.*, antibody). In addition to the attributes already listed, *ERLs* have two key features, both deriving from the use of gold colloids. First, each particle is coated with a large number of reporters (10^3–10^5). The response to an individual binding event is therefore markedly amplified. Second, gold surfaces are readily modified by thiols and disulfides.[35] This chemistry provides a simple, versatile route to surface modification. We add that assays carried out using *ERLs* after refrigerated storage for three months yielded results that differed by no more than 10% from those performed using the freshly prepared material, testifying to the long term stability of the *ERLs*. The following draws out each attribute by discussing the trade-offs in the performance and ease of fabrication for three types of *ERLs* that we have designed and tested to date.

Co-adsorbed, mixed monolayer ERLs. As depicted in Scheme 2, our first version of *ERLs* used co-adsorbed antibodies and reporters.[16] In this case, the antibody was simply adsorbed on the surface, while the reporter chemisorbed as a thiolate. While successful in the concurrent detection of rat and rabbit IgG, data indicated that a small amount of weakly adsorbed antibody may desorb from one *ERL* and re-adsorb on the second *ERL* in the two-component *ERL* suspension. Thus, the "crosstalk" between the *ERLs* in the labelling suspension for a multiplexed assay led to a spectral signature akin to non-specific adsorption. Furthermore, this pathway was occasionally challenged by problems with particle aggregation, which may also be caused by the partial loss of the protein coating. Alternative designs were therefore investigated to address these issues.

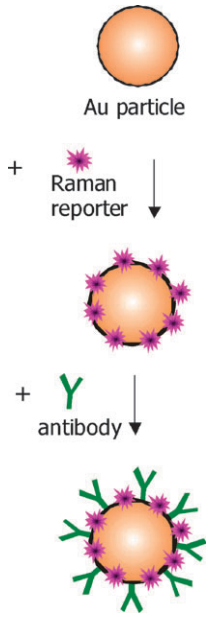

Scheme 2 *ERLs* based on co-adsorption of antibodies and reporters.

ERLs with a bifunctional coating. Scheme 3 illustrates the use of a bifunctional reporter that has a large scattering cross-section and a reactive moiety to covalently couple to an antibody to prevent crosstalk. To this end, 5,5′-dithiobis(succinimidyl-2-nitrobenzoate) (DSNB), the most effective of those prepared and tested, was designed to have the following properties. First, DSNB contains an aromatic nitro group which has a large scattering cross-section due to the symmetric nitro stretch ($\nu_s(NO_2)$). Second, its disulfide moiety reacts with gold by cleaving and forming a thiolate adlayer. This structure also places the nitro group in close proximity with the particle to address the sharp decay in the enhanced electric field as the distance from the surface increases.[43–45] Since each particle is fully covered with the DSNB-derived adlayer, this strategy

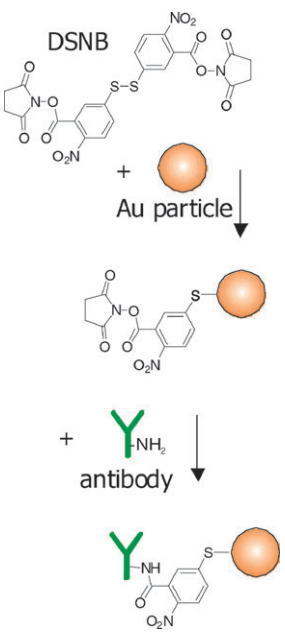

Scheme 3 *ERLs* based on bifunctional coatings.

"squeezes" as much signal as possible from the *ERLs*. Third, the succinimidyl groups of DSNB are used to covalently tether antibodies to the particles.[33,46,47] In total, this scheme improved particle stability and lowered the limit of detection. Using this type of *ERL*, we realized femtomolar detection of f-PSA directly in human serum.[25]

Synthesis and characterization of bifunctional ERLs. DSNB was synthesized in one step *via* carbodiimide coupling in a mixture of 5,5′-dithiobis(2-nitrobenzoic acid), dicyclohexylcarbodiimide, and *N*-hydroxysuccinimide in THF. Prior to exposure to DSNB, the pH of the particle suspension (80 nm diameter, 1.1×10^{10} particles mL^{-1} or 60 nm diameter, 2.6×10^{10} particles mL^{-1}, purchased from Ted Pella) was adjusted with borate buffer (pH 8.5). This pH is above the isoelectric point (pI) of the antibody, which inhibits aggregation of the labelled particles, and deprotonates the amines of the antibody, which favours coupling with the succinimidyl ester of DSNB.

As part of an assessment of the modification process, the Raman spectrum of DSNB was measured before and after nanoparticle immobilization. The powder spectrum is dominated by $\nu_s(NO_2)$ at 1341 cm^{-1}. Other strong bands in the spectrum are at 1568 cm^{-1}, assigned to an aromatic ring mode (8a), and at 1066 cm^{-1}, probably a succinimidyl N–C–O stretch overlapping with aromatic ring modes. Importantly, many of the bands are present in the spectrum after chemisorption to the gold particles, though some undergo a small change in position due to interactions between neighboring adsorbates and with the gold surface. These results confirm that the particles have been effectively modified. While bifunctional *ERLs* provided excellent assay results, this approach nevertheless requires synthesis of the bifunctional reporters.

Mixed monolayer ERLs with antibody linker. Scheme 4 combines the advantages of the previous two designs, resulting in detection levels comparable to the DSNB-based reporter

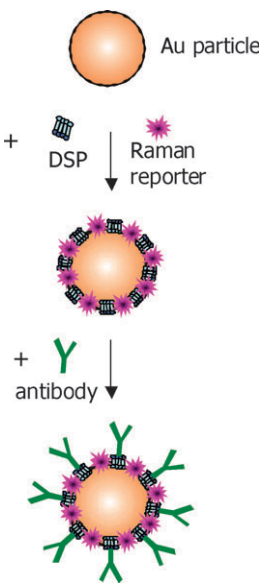

Scheme 4 *ERLs* based on a mixed monolayer of antibody linkers and reporters.

while offering a much more facile route to modification.[26] In this instance, the particles are modified with two different thiolates, each from commercial sources. One thiolate is derived from the bifunctional compound DSP, which has disulfide and succinimidyl groups like DSNB but is an inherently weak scatterer. Thus, the second thiolate is selected to have a large Raman cross-section (*e.g.*, 4-nitrobenzenethiol). This design therefore embodies the attributes of our bifunctional reporters. Moreover, it greatly facilitates the production of different *ERLs*, referred to as mixed-monolayer *ERLs*, for multianalyte assays by using different antibodies that are paired with spectroscopically distinguishable, commercially available reporters.

Synthesis of mixed monolayer ERLs. These *ERLs* are prepared by first spontaneously adsorbing the mixed monolayer. Excess reactants are then removed by centrifuging at 2000*g* and decanting the supernatant. The particles are re-suspended in buffer and incubated with antibody, followed by blocking with BSA. After again removing the reactants by centrifugation, the suspension is adjusted to a physiological NaCl concentration and passed through a 0.22 μm filter to remove any large aggregates.

Optimization. Previous work showed that the pH and ionic strength of the *ERL* suspension play key roles in stabilizing the suspension in each step of the preparation.[16,24] The importance of pH is due to the pI of the antibody. A pH above the pI minimizes *ERL* aggregation. In addition, amide formation is controlled by pH because the linkage reaction proceeds through deprotonated amines. Flocculation tests are used in each step to evaluate the impact of changes in preparative conditions.

Another part of the process identifies the optimal blocking agent. Since the signal from blank samples defines the observed limit of detection, non-specific binding by *ERLs* to the capture surface degrades assay performance. We therefore carry out trial-and-error tests with a panel of blocking agents (*e.g.*, BSA, HSA, Superblock, and casein) to determine the best blocker for a given set of assay conditions.

Characterization

Gold nanoparticles. We have found that gold nanoparticles from many commercial sources have a wide range of particle diameters; some also have large batch-to-batch variations. Since size and shape control the particle plasmon resonance frequency,[17,18] constancy is paramount to the fabrication of *ERLs* and the ability to realize a quantitative and reproducible assay. We have adopted two measures to address this variability by characterizing the size and shape distributions of each new batch of particles with TEM and AFM. For example, our TEM measurements of as-received gold nanoparticles with a vendor-specified diameter 60 nm (±8%) indicated an average diameter of 63.4 nm (±8%).

Fig. 4 and its inset demonstrate the utility of AFM as a tool for particle size characterization by presenting a series of histograms generated from images of different sized gold particles distributed on a gold-coated glass slide.[30] Sizes were measured by using particle height as the determinant because tip convolution effects can distort the lateral dimensions of

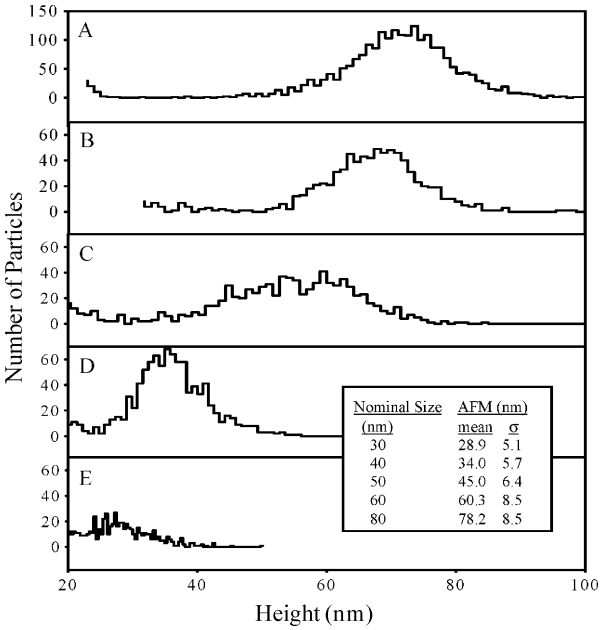

Fig. 4 Histograms from the AFM particle size distribution analyses: 80 nm (A); 60 nm (B); 50 nm (C); 40 nm (D); and 30 nm (E). Reproduced with permission from ref. 30.

nanometrically sized objects. Since there was no clear gap between the background and particle height distribution for the 30 nm particles, this specific analysis was performed by assuming a symmetric peak profile.

The inset summarizes the particle analysis results. In general, the AFM-determined particle sizes are close to, but smaller than vendor specifications. The largest relative differences occur with the 40 and 50 nm particles; both were more than 10% smaller than specified. We also occasionally found that some batches of particles contained a number of much larger particles, which led to the use of a filtering step (0.22 μm filters).

Flocculation. We often use flocculation to test the effectiveness of antibody coupling.[24] A recent example of results is summarized by the extinction spectra in Fig. 5 from work in the development of *ERLs* for feline calicivirus (FCV), a simulant for the human calicivirus known as norovirus. This study systematically varied the amount of anti-FCV monoclonal antibody (mAb) added to borate-buffered suspensions of 60 nm gold and monitored aggregation upon the addition of NaCl to physiological concentration (150 mM).[24]

Fig. 5 shows that the as-received suspension has an extinction maximum at 535 nm, consistent with the location of the plasmon resonance of isolated gold particles with an average diameter of 60 nm.[48] The precipitation of particles from the solution modified with 5 μg of anti-FCV mAb is revealed by the large decrease in the strength of this band. The broadening and shift to longer wavelengths is also diagnostic of aggregation. Increases in the amount of mAb, however, narrows and increases the band, which when coupled with expectations from the dilution that results from sample manipulation, is diagnostic of stable colloidal suspensions. Moreover, there was no observable precipitate for samples stored for several

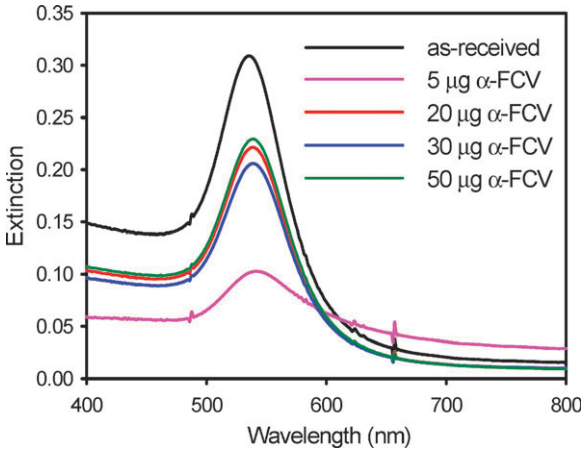

Fig. 5 UV-visible extinction spectra of colloidal gold (60 nm) before and after mixing with anti-FCV mAb (5–50 μg) for 1 h, followed by addition of NaCl to a final concentration of 150 mM NaCl. Reprinted with permission from ref. 24. Copyright 2005 American Chemical Society.

weeks. Flocculation tests are therefore another key component in *ERL* optimization.

Zeta potential. Zeta potentials (ζ) present another measure for assessment of particle stability throughout the preparative process. The sign and magnitude of ζ is directly proportional to the sign and magnitude of the surface charge density of a particle,[49] and are indicators of stability with respect to aggregation. For example, 60 nm Au nanoparticles that are coated with the negatively charged capping agent citrate have ζ-values of about −37 mV. After modification with DSNB and immobilization of an IgG antibody, ζ is roughly −15 mV, indicating a decrease in surface charge density. We typically find values greater than 10–20 mV (independent of sign) sufficient for excellent particle stability (shelf life of at least several months).

Role of plasmon interactions. As part of our investigations of this assay strategy, we also attempted to develop an assay by changing the underlying gold substrate to a low fluorescence glass material. However, the resulting signal strengths were much weaker than those observed when using a gold capture substrate. This result led to an investigation of the possible role of the metal substrate.[39] The impact of the metal substrate on the spectroscopic properties of nanoparticles is illustrated in Fig. 6. Upon immobilization, the particle extinction maximum shifts to longer wavelengths. Qualitatively, these differences are consistent with theories that take into account the electromagnetic coupling between the plasmons of the particle and underlying gold substrate.[50] The extent of coupling is dependent on the ratio of the particle diameter, d, to the separation, a, between the particle and substrate. As such, the location of the extinction maximum will occur at larger values (*i.e.*, more coupling) as d increases at constant a. Our results, based on experimental and theoretical perspectives,[39] agree with this expectation, and confirm the importance of substrate coupling on the observed response. These results showed a maximum in scattering enhancement factor when the wavelength of the plasmon resonance of the immobilized particles

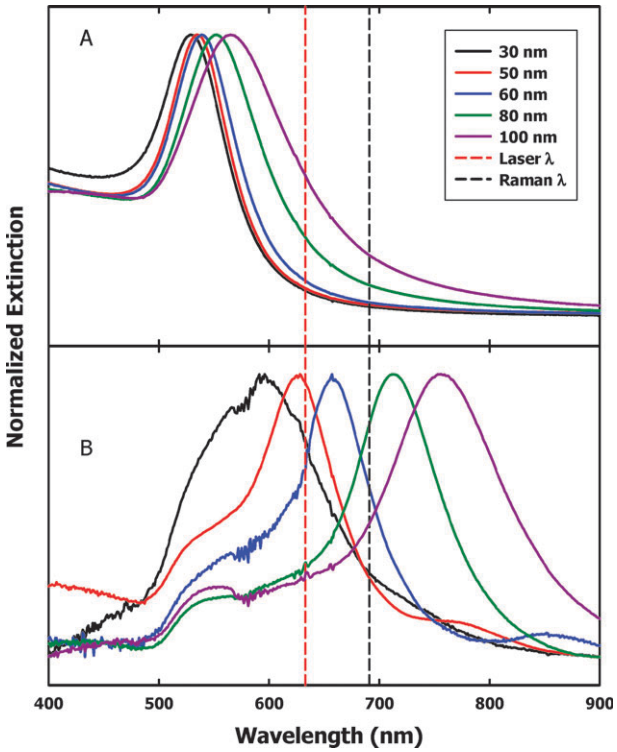

Fig. 6 (A) Extinction spectra of gold colloid suspensions; (B) surface extinction spectra of gold colloids on a gold surface. Adapted and reprinted with permission from ref. 39. Copyright 2006 American Chemical Society.

fell between that of the laser and the Raman band. This maximum occurred for 60 nm particles on gold substrates and 80 nm gold particles on silver substrates (Fig. 7).

SERS measurements

The final step in the assay quantifies the antigen by measuring the response generated by captured *ERLs*. Much of our work employs a low-cost (~$15 K), field-deployable system, the NanoRaman I fibre-optic-based Raman system (Fig. 8, Concurrent Analytical). This system uses a HeNe laser (632.8 nm) as the excitation source. The spectrograph consists of an f/2.0

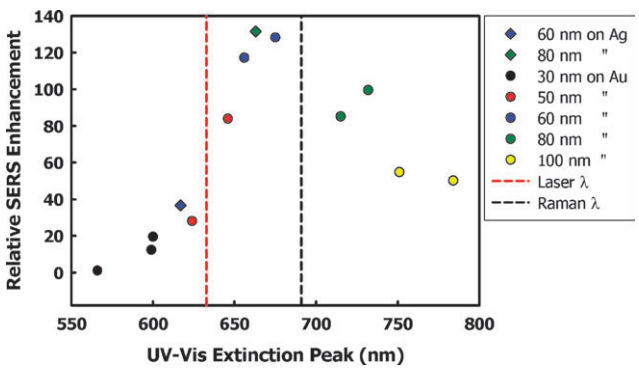

Fig. 7 SERS enhancement for different gold nanoparticle diameters relative to enhancement by 30 nm diameter particles, plotted as a function of the wavelength of maximum extinction. Adapted and reprinted with permission from ref. 39. Copyright 2006 American Chemical Society.

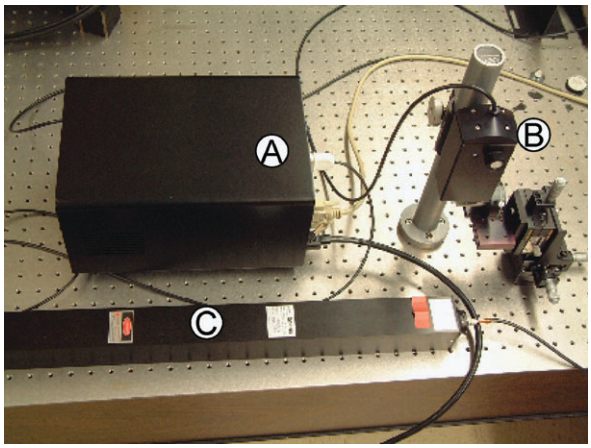

Fig. 8 SERS instrument: (A) spectrometer; (B) fibre optic probe; and (C) HeNe laser.

Czerny-Turner imaging spectrometer (6–8 cm^{-1} resolution) and a Kodak 0401E CCD, thermoelectrically cooled to 0 °C. The laser light is focused to a 25 μm spot on the substrate at normal incidence using an objective with a numerical aperture of 0.65; the power at the sample is ~3 mW. The same objective collects the scattered radiation. Spectra can be acquired over a range of integration times, typically in only a few seconds. As will be shown, this simple system was used to measure f-PSA at femtomolar levels.

Features of the SERS immunoassay platform

To briefly summarize, our immunoassay platform has several noteworthy features. First, enhancements are reproducibly and quantitatively controlled by the size and shape of the nanoparticle, which eliminates the need for a reproducibly roughened capture surface. Moreover, the underlying TSG, which is atomically flat and therefore inactive as an enhancing material, can also be prepared with a high level of reproducibility.[31]

Second, the *ERL* design minimizes the distance between the particle surface and reporters. This aspect is significant because the enhancement of the electric field varies inversely with the 10th power of the distance from the surface.[43] This decay also has another important consequence: there is no observable response attributable to the antibody coating.[16] This result reflects: (1) the gap between the particle and antibody that is enforced by the thickness of the reporter; and (2) the low number of strong scattering modes that is inherent in the structure of most native proteins.

Third, multiplexed analysis can be realized simply by changing the recognition elements on the capture substrate and *ERL* and forming multiple addresses on the capture substrate. This versatility is particularly important in the area of disease detection, which is increasingly relying on the results from a panel of biomarkers rather than a single marker.

Assays

To illustrate the versatility and sensitivity of SERS-based assays, a few examples of work from our laboratory are

detailed for analytes ranging from protein molecules to bacteria.

Femtomolar antigen detection

One of the first applications we investigated with respect to the potential utility of *ERLs* tackled needs in early disease diagnosis, specifically the detection of prostate specific antigen (PSA). Prostate cancer is the second leading cause of cancer-related deaths in adult males in the United States. PSA, a 33 kDa glycoprotein, exists in blood plasma in both complexed and free forms; normal levels are between 4–10 ng mL^{-1}.[51] Assays today distinguish between the different forms of PSA through unreacted epitopes in each complex. The distinction between complexed and free PSA is clinically relevant because the probability of cancer occurrence increases as the percentage of free PSA decreases. Early detection, particularly after radical prostatectomy, is difficult because the low levels of PSA present early in recurrence challenge the detection capabilities of most assays.[52]

In designing this assay, *ERLs* were constructed by coating 30 nm gold particles with a monolayer formed from DSNB. Two different monoclonal antibodies were used, one for the capture substrate and the other for the *ERLs*. Each clone targets a different epitope on f-PSA, which enables formation of the antigen "sandwich." Furthermore, test panel results indicated that a phosphate buffered saline (PBS) rinse buffer (pH 7.5) which contained 0.5% Tween 80 proved highly effective in minimizing nonspecific adsorption of *ERLs*.

The merits of this strategy become evident from inspection of the SERS data in Fig. 9 for an assay of f-PSA spiked in normal human serum.[25] The results, obtained using a 30 s readout time, show: (1) a clear correlation between the strength of $\nu_s(NO_2)$ of the *ERLs* and f-PSA concentration; and (2) a non-detectable level of non-specific adsorption in blank human serum. By defining the limit of detection (LOD) as the response of the blank plus three times its standard deviation, the assay in human serum has a LOD of ~1 pg mL^{-1} (~30 fM). A rough estimate of the number of bound particles (~60), and therefore recognition events, further underscores the ability of this type of assay to detect exceedingly small amounts of antigen, and points to a wide range of opportunities in the application of the readout modality to early disease detection.

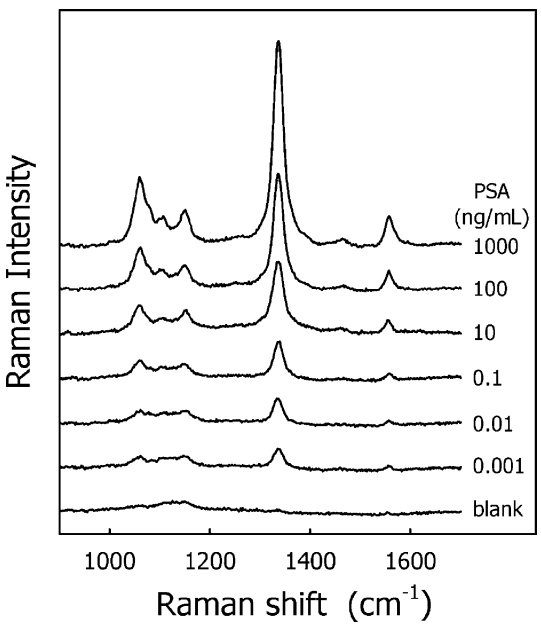

Fig. 9 SERS immunoassay for f-PSA directly from spiked human serum. Spectra (30 s integration times) are offset for clarity. Reprinted with permission from ref. 25. Copyright 2003 American Chemical Society.

Following this work it became evident that larger nanoparticles should provide stronger SERS because their plasmon resonance is more favourably positioned with respect to the laser wavelength (Fig. 7). We therefore switched to using 60 nm diameter particles.

Bacteria detection

We have also been heavily involved in the application of our platform to veterinary medicine by the development of assays for the rapid, low-level detection of viruses.[24] This work, carried out in close collaboration with scientists at the US Department of Agriculture National Animal Disease Center (NADC), was recently extended to pathogenic microorganisms, specifically *Mycobacterium avium* subsp. *paratuberculosis* (MAP).[53,54] MAP is the causative agent of Johne's disease in cattle, and is responsible for the annual loss of several hundred million dollars in worldwide animal production. It has also been implicated as the possible agent in Crone's disease in humans. One of the major obstacles in controlling the spread of this disease is the inability to rapidly detect small amounts of bacteria or other diagnostic markers shed during the subclinical stage of infection. While culturing remains the "gold standard" for MAP detection, it can require 12–14 weeks for incubation.

To address the need for a more rapid assay, we developed a SERS-based method for the detection of MAP in lysate. There is one key feature of this new assay: use of an immobilized layer of a newly created monoclonal antibody that targets a major membrane protein on MAP for construction of the capture substrate and *ERLs*. By correlating the number of MAP bacilli present prior to sonication and the amount of total protein in the resulting sonicate, the detection limit

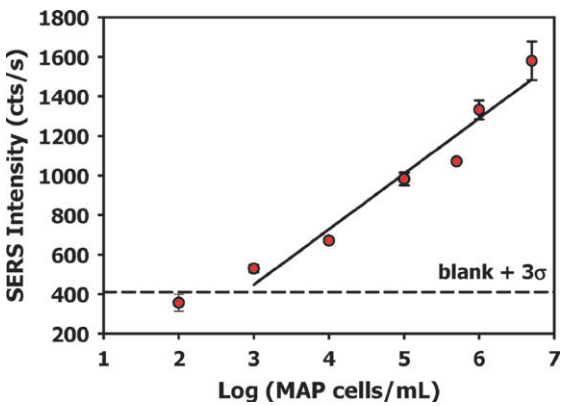

Fig. 10 Calibration curve for MAP spiked in whole milk. Reproduced with permission from ref. 53.

determined for total protein can be translated to the microorganism concentration. These findings, summarized in Fig. 10, yielded an LOD of 1000 MAP mL^{-1} for sonicate spiked in whole milk. This is approaching the levels measured in the subclinical stage of the disease.[53] Moreover, the assay time, which includes sample preparation, antigen extraction, *ERL* incubation, and readout, was under 24 h.

Single gold nanoparticle detection

This section briefly demonstrates the ability to detect individual *ERLs*. It draws on optimizations guided by the results from the noted investigation on both the role of particle size and the separation from the gold substrate on the effectiveness of plasmon coupling.[30] To facilitate the evaluation of individual particles, patterned gold substrates were used to register particle locations *via* AFM, and then interrogated with a Raman (1 μm spot size) microscope.

Fig. 11A and B present AFM topographic images of the patterned gold substrate. Fig. 11B is an expanded image of the substrate location outlined by the dashed lines in Fig. 11A. The bright spots in the images are topographic signatures of the gold particles. The circled areas in Fig. 11B designate regions where SERS measurements were made. Note that region 1 contains a single ERL (80 nm diameter), whereas region 2 is devoid of particles.

The spectroscopic results are given in Fig. 11C and D. Spectral features characteristic of DSNB-coated gold particles are evident in region 1, but not in region 2. Though not shown, additional measurements indicated that all of the particles were SERS active, and the intensities were strongly correlated with particle size.[30] These data demonstrate the ability to detect individual *ERLs*, which, by extension, points to the potential to detect the footprint derived from a single antibody–antigen binding event, *i.e.* the capture of one antigen.

The need for speed

To this point, all the assays have relied on the delivery of antigens and *ERLs* by diffusional mass transport. However, the large sizes of biological targets (Fig. 1) translate to small diffusion coefficients (*e.g.*, 10^{-7} cm^2 s^{-1} for FCV), which can necessitate long incubation times for both the capture and labelling steps. This issue is amplified when attempting to detect antigens at lower and lower levels. Therefore, to take full advantage of the single particle sensitivity of our platform, the development of approaches to reduce incubation times is of fundamental and technological significance.

One path to reduce incubation times arises from the fact that the rate of antigen–antibody binding is often limited by mass transport as opposed to protein–protein recognition.[55,56] Of the many approaches reported in the literature,[57,58] we recently examined the effectiveness of substrate rotation in reducing the time required for the antigen and label binding steps. Although a classic method for accurately controlling the rate of reactant mass transfer in electrochemistry,[59] it has surprisingly few precedents in the bioassay arena. Our work showed, both theoretically and experimentally, that the accumulated surface concentration of bound antigen, Γ_a, is given by eqn (1):

$$\Gamma_a = \frac{2}{\pi^{\frac{1}{2}}} D^{\frac{1}{2}} C_b t^{\frac{1}{2}} + \frac{D^{\frac{2}{3}} C_b}{1.61 V^{\frac{1}{6}}} t\omega^{\frac{1}{2}} \quad (1)$$

where D is the antigen diffusion coefficient, C_b is the bulk antigen concentration, t is incubation time, V is the kinematic viscosity of the solution, and ω is rotation rate. The first right hand term represents the diffusion contribution, whereas the second term defines the hydrodynamically accelerated mass transfer *via* substrate rotation. This equation therefore describes how reactant binding can be manipulated by varying t and, more importantly, ω.

The concept of a rotation-based sandwich assay is given in Fig. 12. One end of a gold-capped rod modified with a capture antibody is lowered into the sample. The rod is then rotated at a controlled rate, which extracts the antigen. After rinsing, the capture substrate is immersed in an *ERL* solution and again rotated at a fixed rate to label the captured antigen. Fig. 13 presents the dose–response curves for the SERS-based detection of rabbit IgG from PBS. When compared to the assay performed under static conditions, the total assay time can be

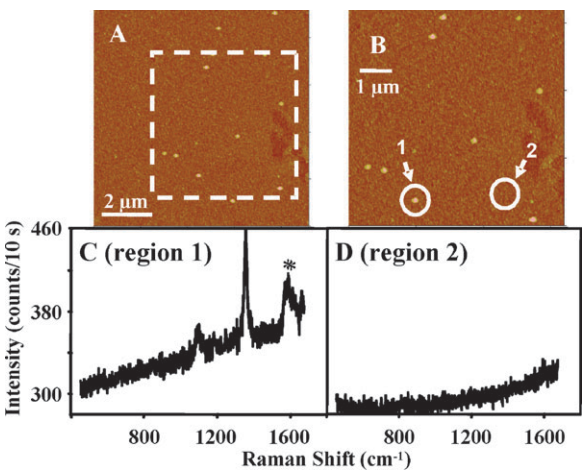

Fig. 11 (A, B) Topographic AFM images of DSNB-coated Au nanoparticles immobilized on aminoethanethiol based self-assembled monolayer (AET SAM) on gold. (C, D) Single-particle Raman spectra of regions 1 and 2 in B. Reproduced with permission from ref. 30.

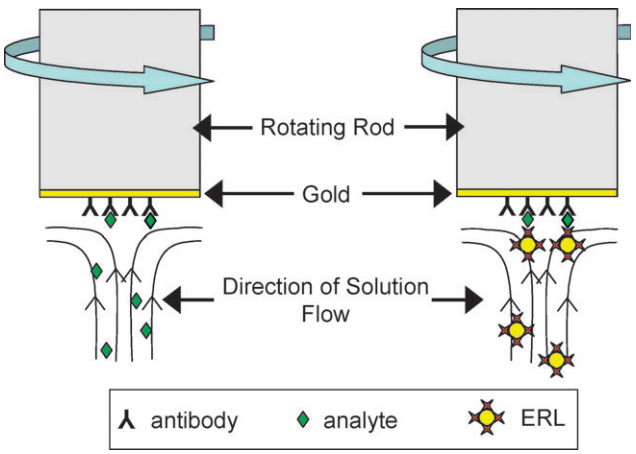

Fig. 12 Schematic of capture and labelling at a rotating capture substrate.

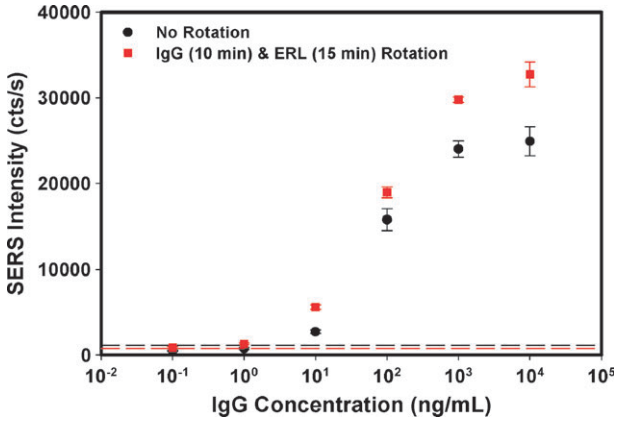

Fig. 13 Dose–response ($\nu_s(NO_2)$ at 1336 cm^{-1}) curves for the detection of rabbit IgG comparing the results for a quiet assay (12 h capture step and 12 h labeling step) to those with rotation at 800 rpm (10 min capture step and 15 min labeling step). The dashed lines are the LOD for each assay. Reprinted with permission from ref. 40. Copyright 2007 American Chemical Society.

reduced from several hours to ~25 min, and this reduction in time is accompanied by a tenfold reduction in detection limit.[40] The improvement in LOD reflects both an increase in signal from the captured antigen and a decrease in nonspecific binding. The latter important finding arises because nonspecific binding is a slower process than specific binding, so accelerated assays allow less time for nonspecific binding to occur.

Conclusions

This review presented a synopsis of our exploration of the potential of SERS-based techniques for high sensitivity detection in a range of heterogeneous immunoassay methodologies. In view of the ability to detect the presence of one captured *ERL*, the continued development of pathways to more effectively exploit this capability represents an unambiguous next step. Advances in new approaches to reduce the time required to capture antigens, particularly from exceedingly dilute samples, will also be of particular importance. From a fundamental viewpoint, there are several intriguing questions, including the role of plasmon coupling between *ERLs* and the underling metal of the capture substrate, as well as the shape manipulation of *ERLs* for even larger enhancements. We believe that these developments will move SERS-based assays center-stage in the world of diagnostics in the very near future.

Acknowledgements

The authors gratefully acknowledge numerous insightful discussions with past and present members of our research group, J. Ni, J. O'Brien, J. Kenseth, V. Jones, D. Grubisha, H.-Y. Park, J. Driskell, K. Kwarta, B. Yakes, J. Uhlenkamp, and N. Grubor, and our colleagues J. Ridpath, J. Neill, J. Bannantine, R. Shinar, and C. Schoen. We also gratefully recognize support from the USDA and National Animal Disease Center, DARPA-CEROS, NIH, the Biodesign Institute at Arizona State University, and the Institute for Combinatorial Discovery and Ames Laboratory, USDOE, Iowa State University.

References

1 http://www.path.cam.ac.uk/~mrc7/igs/migg2a.html.
2 P. A. Pesavento, N. J. MacLachlan, L. Dillard-Telm, C. K. Grant and K. F. Hurley, *Vet. Pathol.*, 2004, **41**, 257.
3 http://johnes.org/general/_EM_scanning.html, Johne's Testing Center, School of Veterinary Medicine, University of Wisconsin.
4 *Immunoassay*, ed. E. P. Diamandis and T. K. Christopoulos, Academic Press, San Diego, 1996.
5 D. Long, *The Raman Effect: A Unified Treatment of the Theory of Raman Scattering by Molecules*, Wiley, New York, NY, 2002.
6 M. Fleischmann, P. J. Hendra and A. J. McQuillan, *Chem. Phys. Lett.*, 1974, **26**, 163.
7 D. L. Jeanmaire and R. P. Van Duyne, *J. Electroanal. Chem. Interfacial Electrochem.*, 1977, **84**, 1.
8 W. E. Doering and S. M. Nie, *J. Phys. Chem. B*, 2002, **106**, 311.
9 K. Kneipp and H. Kneipp, *Appl. Spectrosc.*, 2006, **60**, 322a.
10 G. C. Schatz and R. P. Van Duyne, *Surf. Sci.*, 1980, **101**, 425.
11 K. Kneipp, H. Kneipp, I. Itzkan, R. R. Dasari and M. S. Feld, *Chem. Rev.*, 1999, **99**, 2957.
12 R. L. Garrell, *Anal. Chem.*, 1989, **61**, 401A.
13 M. Moskovits, *Rev. Mod. Phys.*, 1985, **57**, 783.
14 T. Vo-Dinh, *TrAC, Trends Anal. Chem.*, 1998, **17**, 557.
15 K. L. Kelly, E. Coronado, L. L. Zhao and G. C. Schatz, *J. Phys. Chem. B*, 2003, **107**, 668.
16 J. Ni, R. J. Lipert, G. B. Dawson and M. D. Porter, *Anal. Chem.*, 1999, **71**, 4903.
17 C. Burda, X. B. Chen, R. Narayanan and M. A. El-Sayed, *Chem. Rev.*, 2005, **105**, 1025.
18 C. J. Murphy, T. K. San, A. M. Gole, C. J. Orendorff, J. X. Gao, L. Gou, S. E. Hunyadi and T. Li, *J. Phys. Chem. B*, 2005, **109**, 13857.
19 K. Faulds, W. E. Smith and D. Graham, *Analyst*, 2005, **130**, 1125.
20 T. E. Rohr, T. Cotton, N. Fan and P. J. Tarcha, *Anal. Biochem.*, 1989, **182**, 388.
21 X. Dou, T. Takama, Y. Yamaguchi and H. Yamamoto, *Anal. Chem.*, 1997, **69**, 1492.
22 S. P. Mulvaney, M. D. Musick, C. D. Keating and M. J. Natan, *Langmuir*, 2003, **19**, 4784.
23 D. O. Ansari, D. A. Stuart and S. Nie, *Proc. SPIE–Int. Soc. Opt. Eng.*, 2005, **5699**, 82.
24 J. D. Driskell, K. M. Kwarta, R. J. Lipert, M. D. Porter, J. D. Neill and J. F. Ridpath, *Anal. Chem.*, 2005, **77**, 6147.
25 D. S. Grubisha, R. J. Lipert, H. Y. Park, J. Driskell and M. D. Porter, *Anal. Chem.*, 2003, **75**, 5936.
26 H.-Y. Park, *Chip-scale Bioassays Based on Surface-enhanced Raman Scattering: Fundamentals and Applications*, Iowa State University, Ames, 2005.
27 S. Xu, X. Ji, W. Xu, X. Li, L. Wang, Y. Bai, B. Zhao and Y. Ozaki, *Analyst*, 2004, **129**, 63.
28 X. Zhang, M. A. Young, O. Lyandres and R. P. Van Duyne, *J. Am. Chem. Soc.*, 2005, **127**, 4484.
29 Y. C. Cao, R. Jin and C. A. Mirkin, *Science*, 2002, **297**, 1536.
30 H.-Y. Park, R. J. Lipert and M. D. Porter, *Nanosensing: Materials and Devices (Proceeding of SPIE)*, SPIE, Bellingham, WA, 2004, p. 464.
31 D. Stamou, D. Gourdon, M. Liley, N. A. Burnham, A. Kuik, H. Vogel and C. Duschl, *Langmuir*, 1997, **13**, 2425.
32 N. M. Grubor, R. Shinar, R. Jankowiak, M. D. Porter and G. J. Small, *Biosens. Bioelectron.*, 2004, **19**, 547.
33 P. Wagner, M. Hegner, P. Kernen, F. Zaugg and G. Semenza, *Biophys. J.*, 1996, **70**, 2052.
34 B. L. Frey and R. M. Corn, *Anal. Chem.*, 1996, **68**, 3187.
35 J. C. Love, L. A. Estroff, J. K. Kriebel, R. G. Nuzzo and G. M. Whitesides, *Chem. Rev.*, 2005, **105**, 1103.
36 B. Vaidya, J. H. Chen, M. D. Porter and R. J. Angelici, *Langmuir*, 2001, **17**, 6569.
37 H. Van Ryswyk, E. D. Turtle, R. Watson-Clark, T. A. Tanzer, T. K. Herman, P. Y. Chong, P. J. Waller, A. L. Taurog and C. E. Wagner, *Langmuir*, 1996, **12**, 6143.
38 Y. Dong and C. Shannon, *Anal. Chem.*, 2000, **72**, 2371.

39 J. D. Driskell, R. J. Lipert and M. D. Porter, *J. Phys. Chem. B*, 2006, **110**, 17444.
40 J. D. Driskell, J. M. Uhlenkamp, R. J. Lipert and M. D. Porter, *Anal. Chem.*, 2007, **79**, 4141.
41 H. Y. Park, J. D. Driskell, K. M. Kwarta, R. J. Lipert, M. D. Porter, C. Schoen, J. D. Neill and J. F. Ridpath, *Top. Appl. Phys.*, 2006, **103**, 427.
42 M. D. Porter, J. D. Driskell, K. M. Kwarta, R. J. Lipert, J. D. Neill and J. F. Ridpath, *Dev. Biol. (Basel, Switz.)*, 2006, **126**, 31.
43 B. J. Kennedy, S. Spaeth, M. Dickey and K. T. Carron, *J. Phys. Chem. B*, 1999, **103**, 3640.
44 S. L. McCall and P. M. Platzman, *Phys. Rev. B: Condens. Matter Mater. Phys.*, 1980, **22**, 1660.
45 J. Gersten and A. Nitzan, *J. Chem. Phys.*, 1980, **73**, 3023.
46 V. W. Jones, J. R. Kenseth, M. D. Porter, C. L. Mosher and E. Henderson, *Anal. Chem.*, 1998, **70**, 1233.
47 S. D. Duhachek, J. R. Kenseth, G. P. Casale, G. J. Small, M. D. Porter and R. Jankowiak, *Anal. Chem.*, 2000, **72**, 3709.
48 J. A. Creighton, Metal Colloids, , *Surface Enhanced Raman Scattering*, ed. R. K. Chang and T. E. Furtak, Plenum Press, New York, 1982.
49 R. J. Hunter, *Zeta Potential in Colloid Science: Principles and Applications*, Academic Press, New York, NY, 1988.
50 T. Okamoto and I. Yamaguchi, *J. Phys. Chem. B*, 2003, **107**, 10321.
51 T. J. Polascik, J. E. Oesterling and A. W. Partin, *J. Urol. (Hagerstown, MD, U. S.)*, 1999, **162**, 293.
52 A. M. Ward, J. W. F. Catto and F. C. Hamdy, *Ann. Clin. Biochem.*, 2001, **38**, 633.
53 B. J. Yakes, R. J. Lipert, J. P. Bannantine and M. D. Porter, *Clin. Vaccine Immunol.*, 2008, **15**, 227.
54 B. J. Yakes, R. J. Lipert, J. P. Bannantine and M. D. Porter, *Clin. Vaccine Immunol.*, 2008, **15**, 235.
55 A. R. Frackelton and J. K. Weltman, *J. Immunol.*, 1980, **124**, 2048.
56 D. G. Myszka, T. A. Morton, M. L. Doyle and I. M. Chaiken, *Biophys. Chem.*, 1997, **64**, 127.
57 R. W. Glaser, *Anal. Biochem.*, 1993, **213**, 152.
58 K. L. Ewalt, R. W. Haigis, R. Rooney, D. Ackley and M. Krihak, *Anal. Biochem.*, 2001, **289**, 162.
59 A. J. Bard and L. R. Faulkner, *Electrochemical Methods: Fundamentals and Applications*, John Wiley & Sons, New York, NY, 2001.